

THE UNIVERSITY of EDINBURGH

Edinburgh Research Explorer

An integrated expression atlas of miRNAs and their promoters in human and mouse

Citation for published version:

de Rie, D & The FANTOM Consortium 2017, 'An integrated expression atlas of miRNAs and their promoters in human and mouse' Nature Biotechnology, vol. 35, no. 9, pp. 872-878. DOI: 10.1038/nbt.3947

Digital Object Identifier (DOI):

10.1038/nbt.3947

Link: Link to publication record in Edinburgh Research Explorer

Document Version: Peer reviewed version

Published In: Nature Biotechnology

General rights

Copyright for the publications made accessible via the Edinburgh Research Explorer is retained by the author(s) and / or other copyright owners and it is a condition of accessing these publications that users recognise and abide by the legal requirements associated with these rights.

Take down policy The University of Edinburgh has made every reasonable effort to ensure that Edinburgh Research Explorer content complies with UK legislation. If you believe that the public display of this file breaches copyright please contact openaccess@ed.ac.uk providing details, and we will remove access to the work immediately and investigate your claim.



1 Ed sum

An atlas of microRNA expression patterns and regulators is produced by deep
sequencing of short RNAs in human and mouse cells.

- 4
- 5
- 6

An integrated expression atlas of miRNAs and their promoters in human and
 mouse

Derek de Rie^{1,2}, Imad Abugessaisa¹, Tanvir Alam³, Erik Arner^{1,4}, Peter Arner⁵, 9 Haitham Ashoor³, Gaby Åström⁵, Magda Babina⁶, Nicolas Bertin^{1,4,7}, A. Maxwell 10 Burroughs^{1,4,8}, Ailsa J. Carlisle⁹, Carsten O. Daub^{1,4}, Michael Detmar¹⁰, Ruslan 11 Deviatiiarov^{1,11}, Alexandre Fort^{1,4}, Claudia Gebhard^{12,13}, Daniel Goldowitz¹⁴, Sven 12 Guhl⁶, Thomas J. Ha¹⁴, Jayson Harshbarger^{1,4}, Akira Hasegawa^{1,4}, Kosuke 13 Hashimoto^{1,4}, Meenhard Herlyn¹⁵, Peter Heutink¹⁶, Kelly J. Hitchens¹⁷, Chung Chau 14 Hon¹, Edward Huang^{18,19}, Yuri Ishizu^{1,4}, Chieko Kai²⁰, Takeya Kasukawa¹, Peter 15 Klinken²¹, Timo Lassmann^{1,4,22}, Charles-Henri Lecellier^{14,23}, Weonju Lee²⁴, Marina 16 Lizio^{1,4}, Vsevolod Makeev^{25,26,27}, Anthony Mathelier¹⁴, Yulia A. Medvedeva^{25,28,29}, 17 Niklas Mejhert⁵, Christopher J. Mungall³⁰, Shohei Noma^{1,4}, Mitsuhiro Ohshima³¹, 18 Mariko Okada-Hatakeyama^{32,33}, Helena Persson³⁴, Patrizia Rizzu¹⁶, Filip 19 Roudnicky¹⁰, Pål Sætrom³⁵, Hiroki Sato²⁰, Jessica Severin^{1,4}, Jay W. Shin^{1,4}, Rolf K. 20 21 Swoboda¹⁵, Hiroshi Tarui^{1,4}, Hiroo Toyoda³⁶, Kristoffer Vitting-Seerup³⁷, Louise Winteringham²¹, Yoko Yamaguchi³⁸, Kayoko Yasuzawa¹, Misako Yoneda²⁰, Noriko 22 Yumoto³³, Susan Zabierowski³⁹, Peter G. Zhang¹⁴, Christine A. Wells^{18,19}, Kim M. 23 Summers^{9,40}, Hideya Kawaji^{1,4,41}, Albin Sandelin³⁷, Michael Rehli^{12,13}, the FANTOM 24

- 25 consortium, Yoshihide Hayashizaki^{4,41}, Piero Carninci^{1,4}, Alistair R. R. Forrest^{#,1,4,21},
- 26 Michiel J. L. de $\text{Hoon}^{\#,1,4}$.
- 27
- 28 ¹Division of Genomic Technologies, RIKEN Center for Life Science Technologies,
- 29 Yokohama, Japan;
- 30 ²Centre for Integrative Bioinformatics (IBIVU), VU University Amsterdam,
- 31 Amsterdam, The Netherlands;
- 32 ³Computational Bioscience Research Center, Computer, Electrical and Mathematical
- 33 Sciences and Engineering Division, King Abdullah University of Science and
- 34 Technology (KAUST), Thuwal, Saudi Arabia;
- ⁴RIKEN Omics Science Center (OSC), Yokohama, Japan[§];
- ⁵Department of Medicine, Karolinska Institutet at Karolinska University Hospital,
- 37 Huddinge, Sweden;
- ⁶Department of Dermatology and Allergy, Charité Campus Mitte, Universitätsmedizin
- 39 Berlin, Berlin, Germany;
- 40 ⁷Cancer Science Institute of Singapore, National University of Singapore, Singapore;
- 41 ⁸National Center for Biotechnology Information, National Library of Medicine,
- 42 National Institutes of Health, Bethesda, Maryland, USA;
- 43 ⁹The Roslin Institute and Royal (Dick) School of Veterinary Studies, University of
- 44 Edinburgh, Edinburgh, UK;
- 45 ¹⁰Institute of Pharmaceutical sciences, Swiss Federal Institute of Technology (ETH)
- 46 Zürich, Zürich, Switzerland;
- 47 ¹¹Institute of Fundamental Medicine and Biology, Kazan Federal University, Kazan,
- 48 Russia;

- ¹²Department of Internal Medicine III, University Hospital Regensburg, Regensburg,
 Germany:
- ¹³Regensburg Centre for Interventional Immunology (RCI), Regensburg, Germany;
- ¹⁴Department of Medical Genetics, Centre for Molecular Medicine and Therapeutics,
- 53 Child and Family Research Institute, University of British Columbia, Vancouver,
- 54 British Columbia, Canada;
- ¹⁵Melanoma Research Center, The Wistar Institute, Philadelphia, Pennsylvania, USA;
- ¹⁶German Center for Neurodegenerative Diseases (DZNE), Tübingen, Germany;
- ¹⁷Australian Infectious Diseases Research Centre (AID), University of Queensland,
- 58 Brisbane, Queensland, Australia;
- ¹⁸The University of Melbourne Centre for Stem Cell Systems, School of Biomedical
- 60 Sciences, The University of Melbourne, Victoria, Australia;
- ¹⁹Walter and Eliza Hall Institute of Medical Research, Melbourne, Victoria, Australia;
- 62 ²⁰Laboratory Animal Research Center, Institute of Medical Science, The University of
- 63 Tokyo, Tokyo, Japan;
- ⁶⁴ ²¹Harry Perkins Institute of Medical Research, and the Centre for Medical Research,
- 65 University of Western Australia, QEII Medical Centre, Perth, Western Australia,
- 66 Australia;
- 67 ²²Telethon Kids Institute, The University of Western Australia, Subiaco, Western
- 68 Australia, Australia;
- 69 ²³Institute of Molecular Genetics of Montpellier, Montpellier, France;
- 70 ²⁴Department of Dermatology, Kyungpook National University School of Medicine,
- 71 Daegu, South Korea;
- 72 ²⁵Vavilov Institute of General Genetics, Russian Academy of Sciences, Moscow,
- 73 Russia;

²⁶Engelhardt Institute of Molecular Biology, Russian Academy of Sciences, Moscow,

75 Russia;

- 76 ²⁷Moscow Institute of Physics and Technology, Dolgoprudny, Russia;
- ²⁸IMPPC, Institute of Predictive and Personalized Medicine of Cancer, Ctra. de Can
- 78 Ruti, Badalona, Spain;
- ²⁹Institute of Bioengineering, Research Center of Biotechnology, Moscow, Russia;
- 80 ³⁰Environmental Genomics and Systems Biology Division, Lawrence Berkeley

81 National Laboratory, Berkeley, California, USA;

- 82 ³¹Department of Biochemistry, Ohu University School of Pharmaceutical Sciences,
- 83 Koriyama, Japan;
- 84 ³²Laboratory of Cell Systems, Institute for Protein Research, Osaka University,
- 85 Osaka, Japan;
- ³³RIKEN Center for Integrative Medical Sciences, Yokohama, Japan;
- 87 ³⁴Division of Oncology and Pathology, Department of Clinical Sciences, Lund
- 88 University, Lund, Sweden;
- ³⁵Department of Computer and Information Science, Norwegian University of
- 90 Science and Technology, Trondheim, Norway;
- 91 ³⁶Department of Clinical Molecular Genetics, School of Pharmacy, Tokyo University
- 92 of Pharmacy and Life Sciences, Tokyo, Japan.
- 93 ³⁷The Bioinformatics Centre, Department of Biology, and Biotech Research and
- 94 Innovation Centre (BRIC), University of Copenhagen, Copenhagen, Denmark;
- 95 ³⁸Department of Biochemistry, Nihon University School of Dentistry, Tokyo, Japan;
- 96 ³⁹The SKI Stem Cell Research Facility, The Center for Stem Cell Biology and
- 97 Developmental Biology Program, Sloan Kettering Institute, New York, New York,
- 98 United States;

99	⁴⁰ Mater Research Institute - University of Queensland, Translational Research
100	Institute, Brisbane, Australia;
101	⁴¹ RIKEN Preventive Medicine and Diagnosis Innovation Program, Wako, Japan.
102	
103	
104	
105	[§] RIKEN Omics Science Center ceased to exist as of April 1 st 2013 due to RIKEN
106	reorganization.
107	
108	# Correspondence to Michiel de Hoon (michiel.dehoon@riken.jp) and Alistair Forrest
109	(alistair.forrest@gmail.com)
110	
111	

113 MicroRNAs (miRNAs) are short non-coding RNAs with key roles in cellular 114 regulation. As part of the fifth edition of the Functional Annotation of 115 Mammalian Genome (FANTOM5) project, we created an integrated expression 116 atlas of miRNAs and their promoters by deep sequencing 492 short RNA (sRNA) 117 libraries, with matching Cap Analysis Gene Expression (CAGE) data, from 396 118 human and 47 mouse RNA samples. Promoters were identified for 1,357 human 119 and 804 mouse miRNAs and showed strong sequence conservation between 120 species. We also found that primary and mature miRNA expression levels were 121 correlated, allowing us to use the primary miRNA measurements as a proxy for 122 mature miRNA levels in a total of 1,829 human and 1,029 mouse CAGE 123 libraries. We thus provide a broad atlas of miRNA expression and promoters in 124 primary mammalian cells, establishing a foundation for detailed analysis of 125 miRNA expression patterns and transcriptional control regions.

MicroRNAs¹ (miRNAs) are a class of short (21-23 nt) non-coding RNAs with key roles in a wide range of biological processes including development and differentiation^{2,3}, immunity⁴, reproduction⁵, and longevity⁶. Dysregulation of miRNA expression has been implicated in numerous diseases⁷, including cancer^{8,9}. A detailed characterization of the expression profile of miRNAs across cell types and tissues is a fundamental requirement for understanding the function of miRNAs and their potential role in health and disease.

133

134 MicroRNAs inhibit specific mRNAs by binding to complementary sequences, usually 135 located in the 3' UTR, leading to mRNA destabilization and a reduction in their translation output¹⁰. In the canonical miRNA biogenesis pathway^{1,11}, a primary 136 137 miRNA transcript (pri-miRNA) is cleaved by the endoribonuclease Drosha in the 138 nucleus to excise the precursor miRNA (pre-miRNA), which is exported to the 139 cytoplasm. The pre-miRNA has a characteristic hairpin secondary structure that is 140 recognized and cleaved in the cytoplasm by the endoribonuclease Dicer, releasing the 141 mature miRNA.

142

143 Currently, the miRBase reference database of miRNAs¹² lists 1,881 pre-miRNAs in 144 human; around half (54%) are produced from intergenic non-coding pri-miRNA 145 transcripts, while the remaining 46% are excised from the introns of protein-coding 146 transcripts. A small proportion (6%) of human mature miRNAs annotated in miRBase 147 are located in multiple pre-miRNAs encoded in different genomic loci.

148

Several high-throughput approaches are available to measure the expression levels ofmature miRNAs, including high-throughput qPCR, microarray, and next-generation

151 sequencing methods¹³. Profiling pri-miRNAs, which is more challenging due to their 152 transient character, has been accomplished by RNAseq in cells expressing dominant-153 negative Drosha¹⁴. Additionally, since most pri-miRNAs are produced by RNA 154 polymerase II and therefore have a 5' cap¹¹, they are amenable to Cap Analysis Gene 155 Expression (CAGE) profiling^{15,16}, which identifies the pri-miRNA transcription start 156 site and therefore the promoter region, while directly quantitating the pri-miRNA 157 expression level.

158

159 Here, we analyze 492 sRNA sequencing libraries to evaluate the expression patterns 160 of miRNAs in mammalian cells, with a particular emphasis on human primary cells. 161 Each sRNA library was matched to a CAGE library produced from the same RNA 162 sample, allowing us to create an integrated expression atlas of miRNAs and their 163 promoters. The expression atlas can be accessed through a web interface at 164 http://fantom.gsc.riken.jp/5/suppl/De Rie et al 2017/). This work is part of the fifth 165 edition of the Functional Annotation of Mammalian Genome project (FANTOM5)^{17,18}. 166

167 **Results**

168 Matched miRNA and CAGE expression profiles

169 In FANTOM5, a large collection of human and mouse primary cell types, cell lines, 170 and tissues was profiled by CAGE to identify mRNA and long non-coding RNA 171 transcription start sites and expression levels across a wide variety of biological states¹⁷. Here, as a complementary data set, we produced 293 sRNA sequencing 172 173 libraries using FANTOM5 RNA samples from human primary cells, as well as 87 174 sRNA libraries from RNA samples of six time courses of stimulated human cells¹⁸ 175 (Table 1, S1 & S2). We also incorporated previously produced CAGE and sRNA 176 sequencing libraries generated from human embryonic and induced pluripotent stem cells¹⁹ (Table 1 & S1) in our analysis. In total, our sRNA sequencing data set 177 178 encompassed 121 distinct human cell types. In addition, we produced 6 sRNA 179 sequencing libraries from human tissues, and 42 sRNA libraries from mouse samples 180 (Table 1, S1 & S2). Most sRNA libraries were produced in biological triplicate. A matching CAGE library¹⁷⁻¹⁹ generated from the same RNA sample was available for 181 182 492 of the 500 sRNA libraries analyzed here (Table S3).

183

184 Establishing a robust set of miRNAs

Across the sRNA libraries, expression was confirmed for 98% (1842/1877) of human and 95% (1124/1186) of mouse pre-miRNAs annotated in release 21 of the miRBase database¹². To assess the confidence level of annotated miRNAs, the miRBase curators defined a set of five rules evaluating their secondary structure and expression properties (Table 2), and used these rules to mark 295 human pre-miRNAs as highconfidence annotations¹². Applying these rules to the FANTOM5 sRNA data, we found that 571 human pre-miRNAs satisfied all five high-confidence rules, 224 met

192 four of them, and 1076 violated two or more rules (Figure 1a). The 795 human and 193 502 mouse (Figure S1) pre-miRNAs satisfying at least 4 out of the 5 high-confidence 194 rules were defined as the FANTOM5 robust set, and the remaining 1076 human and 195 684 mouse pre-miRNAs as the permissive set (Table S4 and Table S5). The robust set 196 encompasses 735 human and 438 mouse mature miRNAs, and covers more than 90% of the high-confidence pre-miRNAs in miRBase (Figures S2 and S3), 90% of 197 198 miRNAs well characterized in the scientific literature (Figure S4), as well as 91% 199 (human) and 88% (mouse) of pre-miRNAs included in the manually curated MirGeneDB database²⁰ (Figure S5). 200

201

202 CAGE detects 3' cleavage products of Drosha

203 In zebrafish, the Drosha cleavage site at the 3' end of pre-miRNAs was recently found 204 to be characterized by a distinctive CAGE peak²¹. We similarly observed a CAGE 205 peak immediately downstream of the 3' end of human pre-miRNA loci in the ENCODE CAGE data²², and a slightly wider CAGE peak starting 1 nucleotide 206 downstream in the FANTOM5 CAGE data^{17,18} (Figure 1b, c, human; Figure S6, 207 208 mouse); the discrepancy between the ENCODE and FANTOM5 CAGE data is 209 expected because of differences in the sequencer technologies employed (Figure S7). 210 The ENCODE CAGE peak was found immediately downstream of the 3' end of the 211 pre-miRNA locus (Figure S8) for 19 out of 25 pre-miRNAs with a full-length 212 sequence in the FANTOM4 sRNA sequencing libraries²³, confirming that the CAGE 213 peak marks the Drosha cleavage site. FANTOM5 and ENCODE CAGE tags at the 214 peak were enriched in the nucleus (Figure S9), consistent with processing by Drosha. 215 CAGE peaks were absent at the 3' end of pre-miRNA loci encoding mirtrons (Figure

S10, human; Figure S11, mouse), which are excised by the spliceosomal machinery
instead of by Drosha²⁴.

218

219 To rule out the possibility that these CAGE tags originated from an independent 220 transcript, we analyzed the first nucleotide of the CAGE tags at the Drosha cleavage 221 site. Most CAGE tags originating from a transcription start site have an additional 222 guanine as their first nucleotide, as the 7-methylguanosine cap at the 5' end of 223 transcripts produced by RNA polymerase II can be recognized as a guanine nucleotide 224 during reverse transcription (Figure S7). No such additional guanine nucleotides were 225 found at the Drosha CAGE peak (Figure S12), confirming that the detected RNAs 226 were not due to an independent transcription initiation event. The lack of guanine 227 nucleotide enrichment also suggested that the 3' Drosha cleavage products were 228 uncapped RNAs that were nonetheless observed to some extent in the CAGE library 229 due to their cellular abundance. Alternatively, these RNAs may have a 230 hypermethylated cap, as previously found for small nucleolar RNAs (snoRNAs) produced by excision from a host gene transcript²⁵: no additional guanines are found 231 232 as the first nucleotide of CAGE tags mapping to the 5' end of snoRNAs (Figure S12), 233 as hypermethylation of the cap prevents base-pairing during reverse transcription.

234

Excluding mirtrons, about half of the robust pre-miRNAs had a significant (P < 0.05) Drosha CAGE peak (52%, human, Figure 1a; 64%, mouse, Figure S1; see Methods for details). This percentage decreased from 56% for human pre-miRNAs satisfying all five of the miRBase high-confidence criteria to 37% if one of the criteria was violated, while only 7% of miRNAs in the permissive set had a Drosha CAGE peak (Figure 1a). Similar results were obtained for mouse (Figure S1). The analysis of Drosha CAGE peaks thus provided independent support for the stringency of the
selection criteria used to define the FANTOM5 robust and permissive set of miRNAs.

244 Discovery of candidate novel miRNAs

245 To discover potential miRNAs that had not been described previously, the miRDeep2 software²⁶ was applied on all unannotated sRNAs (see Methods for details). In total, 246 247 6,543 candidate miRNAs in human (Table S6, S7) and 1,444 in mouse (Table S8, S9) 248 were identified. Most of the candidate miRNAs were lowly expressed, with fewer 249 than 5% of them having sufficient tag counts on both arms of the pre-miRNA to 250 enable a full evaluation of the high-confidence criteria (Table 2). The 282 human and 251 34 mouse candidate miRNAs meeting at least 4 of the 5 high-confidence criteria 252 formed the robust candidate set, while the permissive candidate set consisted of the 253 remaining candidate miRNAs (Table S4 and Figure S13, human; Table S5 and Figure 254 S14, mouse). The robust candidate set comprised 279 (human) and 33 (mouse) unique 255 mature sequences, whereas the permissive candidate set provided an additional 5,826 256 (human) and 1,354 (mouse) mature sequences. Nearly 11% of robust and 5% of 257 permissive human candidate miRNAs had a significant (P < 0.05) Drosha CAGE 258 peak (Figure S13; Figure S14 for mouse). Validation by qPCR of a selection of robust 259 candidate miRNAs identified in monocyte and macrophage libraries confirmed their 260 expression in these cell types in multiple donors (Figure S15, Table S10).

261

The robust candidate set showed good concordance (127/282 or 45%) with the 3,524 putative miRNAs identified recently in a study of tissue- and primate-specific miRNAs²⁷, whereas the permissive candidate set yielded a smaller overlap (352/6,261 or 6%). Few of these putative miRNAs²⁷ had a significant Drosha CAGE peak 266 (258/3,524 or 7%), which may be due to their low expression levels in the samples267 surveyed in FANTOM5.

268

We conclude that the vast majority of canonical, highly expressed miRNAs had already been annotated. However, our analysis also provides evidence of extensive transcription of lowly expressed short RNAs from specific genomic loci.

272

273 Expression variability of miRNAs in human primary cells

274 The cell type dependence of expression of individual miRNAs was evaluated by 275 analyzing the distribution of miRNA abundance across the FANTOM5 primary cells 276 and tissues. First, we assessed various expression normalization strategies, and found 277 that a counts per million (cpm) normalization (i.e., dividing the tag count of each 278 miRNA by the total number of tags mapping to miRNA loci, and multiplying by 279 1,000,000) yielded the best reproducibility between different donors for the same cell 280 type, while maintaining the distinction in expression profile between different cell 281 types (Figure S16; see Methods for details). We then created a miRNA expression 282 table across the FANTOM5 samples for human (Table S11) and mouse (Table S12), 283 using cpm normalization in our further analysis. Figure 2a shows a graphical 284 overview of the human primary cells clustered by their robust miRNA expression 285 profile using Miru²⁸. An interactive heatmap of the expression data is available at

286 <u>http://fantom.gsc.riken.jp/5/suppl/De_Rie_et_al_2017/vis_viewer/#/heatmap.</u>

The expression levels of miRNAs varied greatly and were highly skewed, with on average five miRNAs contributing half of the total miRNA expression in a given library (Figure 2b, human; Figure S17, mouse), whereas most known and candidate miRNAs were lowly expressed (Figure 2c, human; Figure S18, mouse). The extreme distribution of miRNA expression across miRNAs and cell types was confirmed byqPCR (Figure S19).

293

294 Cell ontology analysis

295 A cell type specificity index, analogous to the previously defined tissue specificity index²⁹, was calculated to quantify the cell type specificity of miRNA expression 296 297 across the FANTOM5 collection of primary cell types (Table S13; see Methods for 298 details). Previously described highly cell type specific miRNAs included miR-122-5p, 299 miR-142-5p and miR-302a-5p, which were enriched in hepatocytes, leukocytes, and 300 pluripotent stem cells, respectively (Figure 2d). In contrast, miRNAs such as miR-301 100-5p and miR-29a-3p were broadly expressed but specifically depleted in particular 302 cell types (leukocytes and pluripotent stem cells, respectively; Figure 2d). Candidate 303 miRNAs tended to be restricted to specific cell types, with 80% of the robust 304 candidate set and 96% of the permissive candidate set having a higher cell type 305 specificity index than the median value for robust known miRNAs (Table S13).

306

307 We then calculated the statistical significance of expression enrichment or depletion 308 of each miRNA (Table S13) with respect to cell ontology clusters (Table S14) defined by the FANTOM5 cell ontology annotation^{30,31}, which organizes FANTOM5 samples 309 310 by cell type in a hierarchical framework (see Methods for details). Of miRNAs in the 311 robust set, 54% had enriched expression in their most significant cell ontology cluster, 312 whereas 27% were broadly expressed, with depleted expression in their most 313 significant cell ontology cluster. The remaining 19% were lowly expressed without 314 statistically significant enrichment or depletion in any cell ontology cluster; 315 understanding their functionality may need profiling in further cell types or states.

Pluripotent stem cells were characterized by cell type specific miRNAs, whereas cell type specific depletion of broadly expressed miRNAs was predominantly found in leukocytes. Examples of enriched expression not reported previously included miR-488-5p in neural cells, miR-506-3p in light melanocytes, and miR-205-5p in epithelial cells. MiRNAs previously not reported as broadly expressed included miR-887-3p, which was present in most samples but was depleted in leukocytes.

322

323 Identification of miRNA promoters

324 We developed an automatic pipeline to identify miRNA promoters using Gencode 325 v19 and RefSeq transcripts as candidate pri-miRNAs and the FANTOM5 CAGE data 326 as putative transcription start sites (see Methods for details). This pipeline predicted 327 promoters for 539 robust, 623 permissive, and 3,951 candidate pre-miRNAs in human 328 (Table S15), and for 358 robust, 446 permissive, and 994 candidate pre-miRNAs in 329 mouse (Table S16). Manual curation by two independent annotators confirmed the 330 selected promoter for 512 (95%) robust pre-miRNAs; the computationally selected 331 promoter was corrected for 26 pre-miRNAs and dropped for 1 pre-miRNA. Manual 332 curation furthermore identified the promoter for an additional 196, mostly intergenic, 333 pre-miRNAs, thereby generating the-to our knowledge-largest miRNA promoter 334 collection to date (Table S17, Figure S20a). Across the human robust set, an 335 associated ENCODE RAMPAGE (RNA Annotation and Mapping of Promoters for 336 the Analysis of Gene Expression³²) 5' end was found within 300 base pairs of more 337 than 75% of the FANTOM5 curated promoters both for intergenic and intronic miRNAs, outperforming the miRGen³³, Chang et al.¹⁴, miRStart³⁴, and TSmiR³⁵ 338 339 collections of miRNA promoter annotations (Figure S20b). The median distance 340 between the FANTOM5 annotated miRNA promoter and the associated RAMPAGE 341 5' end was 1 nucleotide, and was thereby closer than any of the existing miRNA 342 promoter annotations (Figure S20c). RACE experiments confirmed that the transcripts 343 generated at the identified promoter extended to the mature miRNA for 6 out of 7 miRNAs (Figure S21, Table S18). RNA-seq data¹⁴ of cells expressing a dominant-344 345 negative Drosha protein provided additional evidence for the FANTOM5 annotated 346 pri-miRNAs, with 483 out of 607 pri-miRNAs (80%) having a 5' end within 300 base 347 pairs of an RNAseq transcript assembly extending to the mature miRNA locus (Figure 348 S22).

349

350 Both in human and in mouse, promoter sequences of intronic and intergenic miRNAs, 351 like those of transcription factor genes, were highly conserved across species 352 compared to the promoter sequences of protein-coding genes and of long non-coding 353 RNAs (Figures 3a and S23, human; Figure S24, mouse). The distance between the 354 transcription start site of the pri-miRNA and the mature miRNA locus was strongly 355 conserved between human and mouse both for intergenic miRNAs and for intronic 356 miRNAs (Figures 3b and S25). While this suggests that pri-miRNA transcripts may 357 have some functional role beyond providing the substrate for pre-miRNA excision, 358 there was no evidence of substantially elevated sequence conservation across species 359 in pri-miRNAs (Figure S26).

360

361 Correlation of mature miRNA and pri-miRNA expression levels

The expression levels of mature miRNAs correlated with the CAGE expression levels of the associated promoter, with comparable correlation values for intergenic and intronic miRNAs (Figure 3c and S27; Table S19). The correlation was substantially higher for highly differentially expressed miRNAs, and exceeded correlations found for previously published^{14,33-35} miRNA promoter annotations (Figure S20d). About 11% of pri-miRNAs in human were polycistronic, containing multiple mature miRNAs with highly correlated expression levels (Figure 3d and S28). Together this suggests that miRNA expression is primarily regulated at the transcriptional level.

370

371 Using the CAGE expression level of the pri-miRNA as a proxy for the mature 372 miRNA expression level, we extended the FANTOM5 miRNA expression atlas to the 373 full breadth of the 1,829 (human) and 1,029 (mouse) libraries in the FANTOM5 CAGE expression compendium¹⁷⁻¹⁹. This allowed us to assess miRNA expression 374 375 also in samples for which only a CAGE library was available, covering an additional 376 49 primary cell types, 245 cell lines, 138 tissue types, and 13 time courses in human, and an additional 48 primary cell types, 1 cell line, 234 tissue types, and 12 time 377 378 courses in mouse. A cell ontology analysis was performed using the CAGE 379 expression pattern of each human pri-miRNA (Tables S15 and S17) across 338 cell 380 ontology clusters (Table S20) encompassing 636 CAGE libraries. This showed 381 enriched expression of mir-202 in gonad, of mir-208a, known to be a key regulator of cardiac function³⁷, in heart, as well as of multiple miRNAs in brain, including mir-382 383 488, mir-556, and mir-885. Lastly, the CAGE data allowed us to measure the 384 individual contribution of each paralog to the expression of miRNAs encoded 385 multiple times in the human genome, providing evidence for differential regulation of 386 paralogs in different cell types and tissues. For example, we found that mir-128-1 was 387 expressed in most samples, while its paralog mir-128-2 was highly enriched in brain 388 (Figure 3e).

389

390 Transcriptional regulation of miRNA expression

391 The accuracy of the predicted miRNA promoter regions was assessed using the Motif Activity Response Analyis (MARA) framework³⁸ (outlined in Figure S29 and 392 393 Methods). Using this framework, the expression levels of mature miRNAs were 394 predicted based on the presence of putative transcription factor binding sites in the 395 identified miRNA promoter region, and compared to the expression levels of the 396 mature miRNAs observed in the sRNA libraries. The prediction accuracy of the 397 FANTOM5 miRNA promoter atlas outperformed those of previously published miRNA promoter annotations^{14,33-35} (Figure S20e). 398

399

400 **Discussion**

401 MicroRNAs are key factors that contribute to cellular regulation by targeting specific 402 transcripts for translational repression or for degradation. Advances in sequencing 403 technology led to an increase in sequencing depth from nearly 1,300 reads per sRNA libraries in the first miRNA atlas³⁹ to nearly 4.4 million reads per library in 404 405 FANTOM5, allowing an accurate measurement of the expression even of lowly 406 expressed miRNAs. These lowly expressed miRNAs may be abundant in a few cells 407 in the population sampled, or in cell types, cell lines, or cellular conditions that are not 408 included in our sample collection. Alternatively, they may be a signature of the 409 ongoing evolution of the human miRNA repertoire. In particular, pervasive transcription of mammalian genomes^{22,40,41} generates a large number of hairpin 410 411 secondary structures, which are prevalently encoded in the genome, that can act as 412 substrates for processing by Drosha in the nucleus and Dicer in the cytoplasm. 413 Whereas the majority of the sRNAs thus generated may be evolutionarily neutral and 414 remain lowly expressed, some of them may provide a selective advantage, develop higher expression levels during evolution⁴², and become fixed in the genome as core 415

miRNAs. Finally, we note that in spite of the breadth and depth of the FANTOM5
sRNA sequencing data, most sRNAs currently annotated as miRNAs failed multiple
high-confidence criteria, and may belong to a different class of short non-coding
RNAs, such as transcription initiation RNAs²³ or DNA damage response RNAs⁴³, or
may be degradation products⁴⁴.

421

422 Compared to existing miRNA expression atlases^{29,39}, the FANTOM5 atlas covers the 423 widest range of normal primary cells, enabling detailed analyses of miRNA 424 expression and their contribution to establishing and maintaining cell type identity. 425 The candidate miRNAs not reported previously were in particular highly cell type 426 specific, and may therefore be missed in miRNA profiling studies in tissues rather 427 than in specific cell types.

428

We found extensive evidence that CAGE peaks observed at the Drosha cleavage site are due to the downstream RNA fragment generated by Drosha processing of the primiRNA. Analysis of these CAGE tags suggested that these RNA fragments do not have a 7-methylguanosine cap, but may instead be uncapped or, alternatively, have a non-canonical cap. For polycistronic pri-miRNAs, such a cap may play a role in preventing rapid degradation of the downstream fragment, which itself may contain miRNAs.

436

The MARA analysis allowed us to predict miRNA expression levels based on the regulatory motifs found in the miRNA promoter region, indicating that transcriptional regulation plays a central role in governing miRNA expression levels. Comparing the promoters of miRNAs, protein-coding genes, and long non-coding RNAs showed similar prevalences of transcription factor binding sites in proximal promoter regions (data not shown), suggesting that the basic mechanisms of transcriptional regulation are largely the same for these three classes of gene products. The identification of miRNA promoter regions as described in this work therefore paves the way for a detailed analysis of the transcriptional regulation of miRNA expression using the same computational and experimental methods that have previously proven their efficacy in the analysis of gene expression.

448 Acknowledgements

449 FANTOM5 was made possible by the following grants: Research Grant for RIKEN 450 Omics Science Center from MEXT to Y.H.; Grant of the Innovative Cell Biology by 451 Innovative Technology (Cell Innovation Program) from the MEXT, Japan to Y.H.; 452 Research Grant from MEXT to the RIKEN Center for Life Science Technologies; 453 Research Grant to RIKEN Preventive Medicine and Diagnosis Innovation Program 454 from MEXT to Y.H. K.V.S and A.S. were supported by the Lundbeck and Novo 455 Nordisk Foundations. A.R.R.F. is supported by a Senior Cancer Research Fellowship 456 from the Cancer Research Trust, funds raised by the MACA Ride to Conquer Cancer, 457 and the Australian Research Council's Discovery Projects funding scheme 458 (DP160101960). Y.A.M. was supported by the Russian Science Foundation, grant 15-459 14-30002. R.D. was supported by the Russian Science Foundation, grant 14-44-460 00022. We would like to thank Lucia Schwarzfischer for technical assistance and 461 Norbert Eichner and Gunter Meister for sequencing RACE products. We would also 462 like to thank GeNAS for data production.

463

464 Authors' contributions

465 P.A., G.Å., M.B., A.J.C., M.D., D.G., S.G., T.J.H., M.H., P.H., K.J.H., C.K., P.K.,

466 W.L., N.M., M.O., M.O.H., P.R., H.S., R.K.S., H.To., M.Y., N.Y., S.Z., P.G.Z., L.W.,

467 Y.Y., C.A.W., K.M.S., A.R.R.F. provided RNA samples; E.A. and C.O.D. selected

468 samples from the FANTOM5 time courses; Y.I., S.N., and H.Ta. produced the sRNA

469 libraries; I.A., M.L., H.K., and T.K. managed the data; D.d.R., M.J.L.d.H., K.V.S.,

- 470 A.M.B., T.A., H.A., A.H., T.L., H.P., C.L., A.M., V.M., M.R. carried out the
- 471 bioinformatics analyses with the help of C.C.H., M.L., K.H., F.R., and J.S.; C.J.M.
- 472 provided the cell ontology; K.M.S. created the Miru visualization; A.F., A.M.,

- 473 A.R.R.F., A.S., C.L., C.A.W., D.d.R., E.H., F.R., H.P., K.V.S., A.M.B., M.J.L.d.H.,
- 474 M.R., N.B., P.S., R.D., V.M., Y.A.M. contributed to the manual miRNA promoter
- 475 annotation; K.Y. and J.W.S. performed the expression validation experiments of
- 476 known miRNAs; E.H. and C.A.W. performed the validation experiments of candidate
- 477 miRNAs; C.G. and M.R. performed the RACE experiments; J.H. created the web
- 478 visualization tool; D.d.R., A.R.R.F. and M.J.L.d.H. wrote the manuscript with the
- 479 help of E.A., A.S., A.M.B., K.M.S., K.V.S., M.R., N.B., P.C., P.S., C.A.W.; A.R.R.F.
- 480 and M.J.L.d.H. designed the study; P.C. and Y.H. supervised the FANTOM5 project.
- 481

482 **Competing financial interests**

483 The authors declare no competing interests.

484

486 **References**

- 487 1. Bartel, D.P. MicroRNAs: genomics, biogenesis, mechanism, and function.
 488 *Cell* 116, 281–297 (2004).
- 489
 2. Shenoy, A. & Blelloch, R.H. Regulation of microRNA function in somatic
 490 stem cell proliferation and differentiation. *Nat. Rev. Mol. Cell Biol.* 15, 565–
 491 576 (2014).
- 492 3. Li, M. & Izpisua Belmonte, J.C. Roles for noncoding RNAs in cell-fate
 493 determination and regeneration. *Nat. Struct. Mol. Biol.* 22, 2–4 (2015).
- 494 4. Mehta, A. & Baltimore, D. MicroRNAs as regulatory elements in immune
 495 system logic. *Nat. Rev. Immunol.* 16, 279–294 (2016).
- 496 5. Hasuwa, H., Ueda, J., Ikawa, M. & Okabe, M. miR-200b and miR-429
 497 function in mouse ovulation and are essential for female fertility. *Science* 341,
 498 71–73 (2013).
- 499 6. Sun, K. & Lai, E.C. Adult-specific functions of animal microRNAs. *Nat. Rev.*500 *Genet.* 14, 535–548 (2013).
- 501 7. Mendell, J.T. & Olson, E.N. MicroRNAs in stress signaling and human
 502 disease. *Cell* 148, 1172–1187 (2012).
- 503 8. Adams, B.D., Kasinski, A.L. & Slack, F.J. Aberrant regulation and function of
 504 microRNAs in cancer. *Curr. Biol.* 24, R762–R776 (2014).
- 505 9. Lin, S. & Gregory, R.O. MicroRNA biogenesis pathways in cancer. *Nat. Rev.*506 *Cancer* 15, 321–333 (2015).
- 507 10. Jonas, S. & Izaurralde, E. Towards a molecular understanding of microRNA508 mediated gene silencing. *Nat. Rev. Genet.* 16, 421–433 (2015).
- 509 11. Ha, M. & Kim, V.N. Regulation of microRNA biogenesis. Nat. Rev. Mol.
- 510 *Cell. Biol.* **15**, 509–524 (2014).

- 511 12. Kozomara, A. & Griffiths-Jones, S. miRBase: annotating high confidence
 512 miRNAs using deep sequencing data. *Nucleic Acids Res.* 42, D68–D73 (2014).
- 513 13. Pritchard, C.C., Cheng, H.H. & Tewari, M. MicroRNA profiling: approaches
 514 and considerations. *Nat. Rev. Genet.* 13, 358–369 (2012).
- 515 14. Chang, T.C., Pertea, M., Lee, S., Salzberg, S.L. & Mendell, J.T. Genome-wide
 516 annotation of microRNA primary transcript structures reveals novel regulatory
 517 mechanisms. *Genome Res.* 25, 1401–1409 (2015).
- 518 15. Kanamori-Katayama, M. *et al.* Unamplified cap analysis of gene expression
 519 on a single-molecule sequencer. *Genome Res.* 21, 1150–1159 (2011).
- 520 16. Takahashi, H., Lassmann, T., Murata, M. & Carninci, P. 5' end-centered
 521 expression profiling using cap-analysis gene expression and next-generation
 522 sequencing. *Nat. Protoc.* 7, 542–561 (2012).
- 523 17. Forrest, A.R.R. *et al.* A promoter level mammalian expression atlas. *Nature*524 507, 462–470 (2014).
- 525 18. Arner, E. *et al.* Transcribed enhancers lead waves of coordinated transcription
 526 in transitioning mammalian cells. *Science* 347, 1010–1014 (2015).
- 527 19. Fort, A. *et al.* Deep transcriptome profiling of mammalian stem cells supports
- a regulatory role for retrotransposons in pluripotency maintenance. *Nat. Genet.*46, 558–566 (2014).
- 530 20. Fromm, B. *et al.* A uniform system for the annotation of vertebrate microRNA
 531 genes and the evolution of the human microRNAome. *Annu. Rev. Genet.* 49,
 532 213–242 (2015).
- 533 21. Nepal, C. *et al.* Transcriptional, post-transcriptional and chromatin-associated
 534 regulation of pri-miRNAs, pre-miRNAs and moRNAs. *Nucleic Acids Res.* 44,
 535 3070–3081 (2015).

- 536 22. Djebali, S. *et al.* Landscape of transcription in human cells. *Nature* 489, 101–
 537 108 (2012).
- 538 23. Taft, R.J. *et al.* Tiny RNAs associated with transcription start sites in animals.
 539 *Nat. Genet.* 41, 572–578 (2009).
- 540 24. Westholm, J.O. & Lai, E.C. Mirtrons: microRNA biogenesis via splicing.
 541 *Biochimie* 93, 1897–1904 (2011).
- 542 25. Matera, A.G., Terns, R.M. & Terns, M.P. Non-coding RNAs: lessons from the
 543 small nuclear and small nucleolar RNAs. *Nat. Rev. Mol. Cell Biol.* 8, 209–220
 544 (2007).
- 545 26. Friedländer, M.R., Mackowiak, S.D., Li, N., Chen, W. & Rajewsky, N.
 546 miRDeep2 accurately identifies known and hundreds of novel miRNA genes
 547 in seven animal clades. *Nucleic Acids Res.* 40, 37–52 (2012).
- 548 27. Londin, E. *et al.* Analysis of 13 cell types reveals evidence for the expression
 549 of numerous novel primate- and tissue-specific miRNAs. *Proc. Natl. Acad.*550 *Sci. USA* 112, E1106–E1115 (2015).
- 551 28. Freeman, T.C., *et al.* Construction, visualisation, and clustering of
 552 transcription networks from microarray expression data. *PLoS Comput. Biol.*553 3, 2032–2042 (2007).
- 554 29. Ludwig, N. *et al.* Distribution of miRNA expression across human tissues.
 555 *Nucleic Acids Res.* 44, 3865–3877 (2016).
- 30. Meehan, T.F. *et al.* Logical development of the cell ontology. *BMC Bioinformatics* 12, 6 (2011).
- 558 31. Lizio, M. *et al.* Gateways to the FANTOM5 promoter level mammalian
 559 expression atlas. *Genome Biol.* 16, 22 (2015).

560	32. Batut, P., Dobin, A., Plessy, C., Carninci, P. & Gingeras, T. High-fidelity
561	promoter profiling reveals widespread alternative promoter usage and
562	transposon-driven developmental gene expression. Genome Res. 23, 169-180
563	(2013).
564	33. Georgakilas, G. et al. DIANA-miRGen v3.0: accurate characterization of
565	microRNA promoters and their regulators. Nucleic Acids Res. 44, D190-D195
566	(2016).
567	34. Chien, C.H. et al. Identifying transcriptional start sites of human microRNAs
568	based on high-throughput sequencing data. Nucleic Acids Res. 39, 9345-9356
569	(2011).
570	35. Guo, Z. et al. Genome-wide survey of tissue-specific microRNA and
571	transcription factor regulatory networks in 12 tissues. Sci. Rep. 4, 5150 (2014).
572	36. Siepel, A. et al. Evolutionarily conserved elements in vertebrate, insect, worm,
573	and yeast genomes. Genome Res. 15, 1034-1050 (2005).
574	37. Ding, J. et al. Trbp regulates heart function through miRNA-mediated Sox6
575	repression. Nat. Genet. 47, 776–783 (2015).
576	38. Suzuki, H. et al. The transcriptional network that controls growth arrest and
577	differentiation in a human myeloid leukemia cell line. Nat. Genet. 41, 553-562
578	(2009).
579	39. Landgraf, P. et al. A mammalian miRNA expression atlas based on small
580	RNA library sequencing. Cell 129, 1401–1414 (2007).
581	40. Carninci, P. et al. The transcriptional landscape of the mammalian genome.
582	Science 309 , 1559–1563 (2005).
583	41. Kapranov, P. et al. RNA maps reveal new RNA classes and a possible
584	function for pervasive transcription. Science 316, 1484–1488 (2007).

- 585 42. Meunier, J. *et al.* Birth and expression evolution of mammalian miRNA genes.
- 586 *Genome Res.* **23**, 34–45 (2013).
- 587 43. Francia, S. *et al.* Site-specific DICER and DROSHA RNA products control
 588 the DNA-damage response. *Nature* 488, 231–235 (2012).
- 589 44. Valen, E. *et al.* Biogenic mechanisms and utilization of small RNAs derived
 590 from human protein-coding genes. *Nat. Struct. Mol. Biol.* 18, 1075–1082
- 591 (2011).
- 592

594 Figure 1: Selection of robust miRNAs and Drosha CAGE peak analysis.

595 (a) Number of miRBase high-confidence rules (Table 2) satisfied by human pre-596 miRNAs annotated in miRBase (n = 1,871). Pre-miRNAs with a statistically 597 significant (P < 0.05) Drosha CAGE peak are shown in orange; mirtrons are shown in 598 yellow. (b) Genomic locus of mir-223 in human with the total number of FANTOM5 599 (blue) and ENCODE (red) CAGE tags as a function of the genomic position of their 600 5' end, showing a Drosha CAGE peak at the 3' end of the pre-miRNA. FANTOM5 601 sRNA reads are shown at the bottom, colored by their read count as defined by the 602 color bar. The exact extent of the pre-miRNA was determined from FANTOM4 fulllength sequencing data²³. (c) Number of CAGE tags as a function of their starting 603 604 position relative to the 3' end of the pre-miRNA, averaged across human pre-miRNAs 605 in the robust set (n = 795). The 3' end of the pre-miRNA was selected as the 3' end of 606 the most prevalent sRNA on the 3' arm of the pre-miRNA in the FANTOM5 sRNA 607 data, with the position indicated as zero corresponding to the first nucleotide 608 downstream of the 3' end of the pre-miRNA.

609

610 Figure 2: Expression profile and cell ontology analysis of mature miRNAs.

(a) Miru²⁸ visualization of FANTOM5 primary cell samples based on their expression 611 612 profile of robust mature miRNAs. (b) Number of most abundant miRNAs 613 contributing at least 50% of the total miRNA expression in each human sRNA library 614 in FANTOM5 (n = 420). (c) Reverse cumulative distribution of the maximum 615 expression across the FANTOM5 samples of human miRNAs in the robust set (n =616 735), permissive set (n = 999), and robust candidate set (n = 279). (d) Examples of 617 miRNAs enriched or depleted in specific primary cell samples. Expression of miR-618 122-5p, miR-142-5p, and miR-302a-5p was enriched in hepatocytes, leukocytes, and 619 pluripotent stem cells, respectively; miR-100-5p and miR-29a-3p were broadly

620 expressed, but depleted in leukocytes and pluripotent stem cells, respectively.

621

622 Figure 3: Analysis of the curated miRNA promoters of miRNAs in the robust set.

623 (a) (left panel) Sequence conservation of the human genome, evaluated as the average phastCons³⁶ score, in the promoter region of non-coding pri-miRNAs (containing 624 625 intergenic mature miRNAs; n = 132), coding pri-miRNAs (containing intronic mature 626 miRNAs; n = 415), transcription factor (TF)-coding transcripts (n = 1.651), other 627 protein-coding transcripts (n = 15,350), and long non-coding RNAs (n = 1,461). The 628 sequence conservation of randomly selected genome regions is shown in gray. The 629 shaded area corresponds to one standard deviation in the estimated mean phastCons 630 score. (right panel) The average sequence conservation at promoter regions of 631 miRNAs was higher than at the promoter regions of non-TF protein-coding genes (Mann-Whitney $P = 2 \times 10^{-16}$, two-sided) and of long non-coding RNAs (Mann-632 Whitney $P = 1 \times 10^{-35}$, two-sided). Error bars correspond to one standard deviation in 633 634 the estimated mean phastCons score. (b) Distance between the transcription start site 635 of the pri-miRNA and the 5' end of the first pre-miRNA is highly correlated between 636 human and mouse both for coding (Spearman r = 0.90; n = 78; Student t = 18.27; P = 2×10^{-29} two-sided) and for non-coding (Spearman r = 0.86; n = 27; Student t = 8.33; 637 638 $P = 1 \times 10^{-8}$ two-sided) pri-miRNAs, suggesting strong conservation of the genomic 639 extent of pri-miRNAs. (c) Expression levels of pri-miRNAs, as measured by CAGE, 640 and mature miRNAs, as measured by sRNA sequencing, were highly correlated both for coding (average Spearman r = 0.25; n = 362; $P = 2 \times 10^{-53}$, Mann-Whitney U 641 test, one-sided) and non-coding (average Spearman r = 0.27; n = 180; $P = 1 \times 10^{-30}$, 642 643 Mann-Whitney U test, one-sided) pri-miRNAs, compared to a background 644 distribution consisting of correlations between randomly paired pri-miRNAs and 645 mature miRNAs. Correlations for polycistronic pri-miRNAs were averaged across the 646 mature miRNAs. (d) Expression levels between mature miRNAs originating from the same pri-miRNA are highly correlated (average Spearman r = 0.74; n = 1,372; P <647 10⁻¹⁰⁰, Mann-Whitney U test, one-sided), compared to a background distribution 648 649 consisting of correlations between mature miRNAs originating from different pri-650 miRNAs. (e) Cell type-dependent expression of miRNA paralogs: While mir-128-1 651 was broadly expressed across most primary cell samples in FANTOM5, its paralog 652 mir-128-2 was enriched in brain samples. (c-d) The box extends from the lower to the 653 upper quartile, with the center line at the median; the whiskers indicate the full range 654 of the data.

655

Table 1.

Origin	Data collection	Number of samples	Number of cell types		
Drimory colla	FANTOM5	293	118	119	
Primary cells	Fort <i>et al.</i> ¹⁹	6	3	119	
ES cells	Fort <i>et al.</i> ¹⁹	6	1		
iPS cells	Fort <i>et al.</i> ¹⁹	6	1		
Tissues	FANTOM5	6	4 tissues		
Time courses	FANTOM5	87	6 tii	me courses	
Total number of sequenced reads: 1,519,621,910					

658 Human sRNA data sets analyzed in this study.

660 **Table 2.**

The miRBase high-confidence rules¹². As a meaningful evaluation of the second, third, and fourth rule relies on accurate knowledge of the position and extent of the mature miRNA on both strands of the pre-miRNA, we evaluated these three rules only if the first rule was satisfied.

1.	\geq 10 tags on each arm of the pre-miRNA, or	
	\ge 100 tags on one arm of the pre-miRNA, with \ge 5 tags on the other arm	
2.	\ge 50% of the tags on each arm of the pre-miRNA have the same 5' end	
3.	0–4 nt overhang at the mature 3' end on each arm	
4.	≥ 60% of nucleotides of the mature sequence on each arm are base-paired	
5.	$\Delta G < -0.2$ kcal/mole/nucleotide	

665

667 Methods

668 Samples and library preparation

669 Short RNA libraries were prepared following the Illumina TruSeq Small RNA Sample 670 Preparation protocol (catalog number RS-200-0012, RS-200-0024, RS-200-0036, RS-671 200-0048) using the same RNA samples from which CAGE libraries were produced previously^{17,18}, as well as one additional RNA sample without a matching CAGE 672 673 library. RNA samples not previously described are listed in Table S2. TruSeq Small 674 RNA Sample Prep Index Sequences were used as bar codes to allow pooling of 675 multiple samples in one library. The short RNA libraries were sequenced using the 676 Illumina HiSeq2000 sequencer in single-read, 50 base mode. The metadata of all 677 FANTOM5 RNA samples, including those used for sRNA sequencing, are available 678 in the FANTOM5 Semantic catalog of Samples, Transcription initiation And 679 Regulators⁴⁵ (SSTAR; http://fantom.gsc.riken.jp/5/sstar). SSTAR sample pages also 680 provide links to the FANTOM5 miRNA expression atlas web interface.

681

682 Data processing

683 We extracted the short RNA sequences from the raw sequences using in-house scripts. We removed linker artifact sequences using TagDust⁴⁶ version 1.13, ribosomal 684 sequences using rRNAdust¹⁷ version 1.00, and filtered against mature tRNAs, 685 686 ribosomal RNA, and 7SL RNA using global alignment. We mapped the remaining 687 sequences using the Burrows-Wheeler Alignment (bwa) tool⁴⁷ version 0.5.9-r16 to 688 genome assembly hg19 (human) or mm9 (mouse), including chromosome Y if the 689 donor was known to be male. Table S3 shows the number of short RNA sequences 690 mapped to the genome for each sample. Two samples had fewer than 100,000 mapped 691 tags and were discarded from the further analysis.

693 Short RNA annotation and filtering

We used release 21 of the miRBase database¹², lifted over to genome assembly hg19 694 695 (human) or mm9 (mouse), as our reference set of known miRNAs. Four pre-miRNAs 696 in human that could not be lifted over to genome assembly hg19 and an additional six 697 human pre-miRNAs that were lifted over to unplaced chromosomes were excluded 698 from the analysis. We annotated all mapped short RNA reads mapping to genomic 699 loci for ribosomal RNA, tRNAs, the RNA component 7SL of the signal recognition 700 particle, small nuclear RNAs, small nucleolar RNAs, small Cajal body-specific RNA, 701 small cytoplasmic RNAs, and piRNAs. We corrected for cross-mapping as described previously⁴⁸, discarding all mappings to unannotated loci if the short RNA sequence 702 703 could be mapped to an annotated locus instead.

704

705 Drosha CAGE peak analysis

706 We calculated the total number of CAGE tags starting at each genomic position across all 1,885 (human) and 1,202 (mouse) FANTOM5 CAGE libraries^{17,18}, as available at 707 708 http://fantom.gsc.riken.jp/5/datafiles/latest/basic/, as well as all 145 human ENCODE data²², 709 CAGE which downloaded we from 710 http://hgdownload.cse.ucsc.edu/goldenpath/hg19/encodeDCC/wgEncodeRikenCage/. 711 We defined the 3' end of the pre-miRNA as the 3' nucleotide of the mature miRNA on the 3' arm of the pre-miRNA; the expected Drosha cleavage site is immediately 712 713 downstream of this nucleotide. For each pre-miRNA in the robust set, we calculated, 714 for each position with respect to the expected Drosha cleavage site, the total number 715 of CAGE tags in the CAGE libraries. We normalized by dividing by the sum over the 716 positions to obtain the CAGE profile with respect to the expected Drosha cleavage

717 site for each pre-miRNA. We then summed the CAGE profiles across the pre-718 miRNAs to obtain the average CAGE profile with respect to the expected Drosha 719 cleavage site. Based on this profile, we selected a 9-basepair window between -2 and 720 +7 base pairs with respect to the expected Drosha cleavage site for the FANTOM5 721 CAGE data, and an 8-basepair window between -2 and +6 base pairs for the 722 ENCODE CAGE data, as the Drosha CAGE peak window for a given pre-miRNA.

723 For each pre-miRNA, we counted the number of CAGE tags with a 5' end within this 724 window, as well as the number of CAGE tags with a 5' end anywhere between the 725 pre-miRNA boundaries. Since CAGE tags tend to occur in clusters on the genome, we 726 expect the distribution of the CAGE tag counts to be heavily overdispersed compared 727 to the Poisson distribution. We therefore used the negative binomial distribution 728 instead, with the dispersion parameter r estimated by fitting the distribution to the 729 number of CAGE tags in any 8- or 9-basepair window on the human or mouse 730 genome. This resulted in a dispersion of 1.856943 and 1.616542 for the FANTOM5 731 human and mouse CAGE data, respectively (using a 9-basepair window), and 732 0.325001 for the ENCODE CAGE data (using a 8-basepair window). Using these 733 dispersion values, we calculated the statistical significance of the FANTOM5 and 734 ENCODE CAGE peaks given the number k of CAGE tags within the window, the 735 number K of CAGE tags within the pre-miRNA, the window size w, as well as the 736 genomic extent L of the pre-miRNA as $I_{p}(k, r)$, where I is the regularized incomplete 737 beta function and $p = \mu / (r + \mu)$, with $\mu = w K / L$ the expected number of tags at the 738 Drosha CAGE peak under the null hypothesis.

For human, we calculated an overall statistical significance value by combining the
FANTOM5 and ENCODE statistical significance into a single *P*-value using Fisher's
method.

742 The relative occurrence of CAGE tags in different subcellular fractionations (Figure

543 S9) and the bias in the first nucleotide of CAGE tags (Figure S12) were evaluated for

744 pre-miRNAs in the robust set with a statistically significant Drosha CAGE peak.

745

746 Identification of candidate novel miRNA

Candidate novel miRNAs were identified using miRDeep 2^{26} , resulting in 7,461 747 748 (human) and 2,034 (mouse) predicted pre-miRNAs, including 918 (human) and 590 749 (mouse) known pre-miRNAs. To avoid predicted miRNAs from failing the miRBase 750 high-confidence rules due to flaws in the predicted secondary structure, we repeated the secondary structure calculation for each predicted miRNA by applying RNAfold⁴⁹ 751 752 version 2.1.2 on the sequence of the precursor miRNA while constraining the 753 structure by allowing nucleotides in each arm of the hairpin to only base-pair to 754 nucleotides in the other arm of the hairpin. In the comparison of the candidate novel miRNAs with the 3,524 tissue- and primate-specific miRNAs published recently²⁷, we 755 756 required the pre-miRNAs to overlap by at least 80%.

757

758 Validation of candidate novel miRNA expression by qPCR

Fresh buffy coat was obtained from the Red Cross following approval from the human
research ethics committee of The University of Melbourne (ethics ID 1646608.1) and
material supply agreement with Red Cross (16-05VIC-21).

Peripheral blood mononuclear cells (PBMC) were isolated from buffy coat using Ficoll hypaque (GE Healthcare, Uppsala, Sweden) as described previously⁵⁰. CD14+ human monocytes were isolated from PBMC using human CD14+ magnetic beads (Milteny Biotec, Sydney, New South Wales, Australia). CD14+ monocytes were differentiated to macrophages in complete RPMI1640 media supplemented with 10% fetal calf serum and 100 ng ml⁻¹ human macrophage colony-stimulating factor (MCSF) (PeproTech, Rehovot, Israel) for 5 days. Suspended cells were removed and
adherent cells were washed with PBS before macrophages were collected.

770 MicroRNAs were isolated from monocytes and macrophages using mirVana miRNA 771 Isolation Kit (Life Technologies, Melbourne, Victoria, Australia) following the 772 manufacturer's protocol. Briefly, cells were lysed in lysis buffer followed by phenol 773 extraction, and miRNAs were isolated from the phenol aqueous phase using a spin 774 column followed by elution in RNase-free water. Following manufacturer's protocol, 775 cDNA synthesis was performed using miScript PCR Starter Kit (Qiagen, Hilden, 776 Germany) by ligating a poly(A) tail to the miRNA followed by reverse transcription 777 in the presence of universal tag. Samples without reverse transcriptase but with all 778 other components were included and used as negative controls.

Forward primers specific to the candidate novel miRNAs were designed using miRprimer⁵¹ (Table S10). Real-time PCR was performed using miScript PCR Starter Kit (Qiagen, Hilden, Germany) and following the manufacturer's protocol. The PCR reaction was set up with the custom-made forward primers and the universal reverse primer supplied with the kit. No-template controls and cDNA samples without reverse transcriptase were included as negative controls. Thermal cycling was performed as suggested by the manufacturer's protocol.

The expression levels of a wide range of miRNAs have been analyzed using our miRNA PCR assay in order to evaluate the sensitivity of the assay and determine the confidence of our results. Short RNAs commonly used as a reference, including RNU6 and let-7a-5p (ref. 52), showed relatively high expression levels. Other miRNAs that are highly conserved in metazoans or known to be expressed in myeloid cells, including miR-191-5p (ref. 53), miR-15a-5p (ref. 54), miR-206 (ref. 55), miR-

792 335-5p (ref. 56) and miR-339-3p (ref. 56), were included and used as positive 793 controls, and showed moderate expression levels. Expression levels of miRNAs 794 reported to be cell markers for other cell types and assumed to be lowly expressed in 795 myeloid cells, including miR-153-3p (ref. 57) and miR-345-5p (ref. 58), were also 796 analyzed in order to determine the detection limit of the assay. Our results 797 demonstrate that the miRNA PCR assay could specifically detect the presence of the 798 target miRNAs, and measure a wide spectrum of expression levels. The expression 799 levels of the selected candidate novel miRNAs fell within the detection spectrum of 800 our miRNA PCR assay, proving the reliability of our results.

801

802 Evaluation of miRNA expression normalization strategies

We counted the number of short RNA sequences with a length between 18 and 25
nucleotides overlapping the mature miRNA loci in each of the primary cell samples.
We then applied the following normalization strategies:

- CPM (counts per million): Divide the count by the sum of counts for mature
 miRNAs in the robust set, and multiply by 1,000,000;
- TMM (trimmed mean of M values): Apply the "calcNormFactors" function in
 edgeR⁵⁹ with method "TMM" to the table of counts;
- RLE (relative log expression): Apply the "calcNormFactors" function in
 edgeR⁵⁹ with method "RLE" to the table of counts;
- DESeq (effective library size): Apply the "estimateSizeFactorsForMatrix"
 function in DESeq⁶⁰ to the table of counts;
- UQ (upper quantile normalization): Divide the count by the sum of the counts
 of the top-25% most abundant miRNAs in each sample;

816

817

٠

UD (upper decile normalization): Divide the count by the sum of the counts of the top-10% most abundant miRNAs in each sample.

818 To evaluate each normalization strategy, we divided the primary cell samples in 819 FANTOM5 into groups (n = 96) of independent donors of the same cell type. For 820 each cell type group, we calculated the variance for each miRNA across the donors. 821 To find the error between different cell types, we first calculated the average 822 expression for each miRNA across donors in each cell type group, and then calculated the difference in the average expression between each pair of cell type groups ($n = \frac{1}{2} \times$ 823 824 $96 \times 95 = 4,560$) for each miRNA. To evaluate the total error, we calculated the mean 825 squared error across miRNAs for each cell type group, as well as the mean squared 826 error across miRNAs for each pair of cell type groups, and took the square root of 827 each to find the root mean square (RMS) with cell type groups and between cell type 828 groups (Figure S16a). We averaged the RMS error over the n = 96 cell type groups, 829 and over the n = 4,560 pairs of cell type groups, and calculated the ratio of the 830 average RMS error within cell types to the average RMS error between cell types 831 (Figure S16b). To evaluate the standard error (Figure S16c), we calculated the mean 832 square error across cell type groups for each miRNA, as well as the mean squared 833 error across pairs of cell type groups for each miRNA, took the square root, and 834 plotted the resulting RMS value for each miRNA against its mean expression level. 835 We then used linear regression to calculate the slope of the RMS error within each 836 cell type and between different cell types as a function of the miRNA expression 837 level. Dividing these two slopes yielded the ratio in RMS error within cell types and 838 between different cell types, normalized by miRNA expression level (Figure S16d).

839

840 Clustering and visualisation of miRNA expression patterns

841 MicroRNAs were clustered based on their expression patterns using the network visualisation and analysis tool Miru²⁸ (http://kajeka.com/miru/miru-about/). The 842 843 Pearson correlation was calculated for each pair of miRNAs. A modified 844 Fruchterman-Rheingold algorithm was used to lay out the network graph in 3-845 dimensional space, in which 502 nodes representing miRNAs were connected by 846 3,369 weighted, undirected edges representing correlations of at least 0.6 between 847 expression patterns. Areas of high connectively and correlation, representing groups 848 of miRNAs with similar expression profiles, were identified using the Markov 849 clustering algorithm (MCL) with an MCL inflation value of 2.2. Clusters were 850 manually annotated based on the cell type or tissue of greatest expression. All nodes 851 in one cluster and the label describing the cluster are shown in the same color. The 852 smallest labeled cluster contains six nodes; for clarity, smaller clusters have not been 853 labeled but can be identified by groups of nodes of the same color.

854

855 Validation of miRNA expression quantitation by qPCR

Expression of selected miRNAs was measured using the TagMan[®] MicroRNA Assay 856 857 (Applied Biosystems) according to its protocol. RNA samples 11544, 11624, 11705 858 (CD19+ B cells, donor1, 2, and 3), 11269, 11346, 11418 (dermal fibroblast donor1, 2, 859 and 3), 12626 (H9 embryonic stem cells), and 11523, 11603, 11684 (hepatocyte 860 donor1, 2, and 3) (Table S3) were used after confirmation of the RNA quality by 861 measuring the RIN value using a TapeStation and the 260/280 and 260/230 ratios 862 using NanoDrop. The Ct values obtained were normalized against the Ct value of 863 small nucleolar RNA SNORD48.

864

865 Cell type specificity index

Following the definition of the tissue specificity index (TSI)²⁹, we define the cell type specificity index of miRNA *j* as

868
$$\operatorname{index}_{j} = \frac{1}{N-1} \sum_{i=1}^{N} \left(1 - \frac{x_{j,i}}{\max_{j'} x_{j,i'}} \right)$$

where *N* is the number of primary cell types in FANTOM5, and $x_{j,i}$ is the expression in counts-per-million of miRNA *j* in cell type *i*, averaged over independent donors.

871

872 Guide strand selection

For each pre-miRNA, we designated the hairpin arm with the highest expression level (in counts-per-million) in any of the FANTOM5 samples as the guide strand, and refer to the opposite arm as the passenger strand.

876

877 Cell ontology analysis

We used the FANTOM5 cell ontology^{30,31} to create cell ontology clusters (Tables S14 878 879 and S20). We performed a likelihood-ratio test comparing the expression data 880 between the samples in each cell ontology cluster and the background, consisting of 881 all other samples listed in Tables S14 and S20, modeling the tag counts by a negative 882 binomial distribution. For each miRNA, we selected the three cell ontology terms for 883 which the expression in the cell ontology cluster compared to the background was 884 statistically most significantly higher, and the three cell ontology terms for which the 885 expression in the cell ontology cluster compared to the background was statistically 886 most significantly lower. The *P*-values listed in Tables S13, S15, and S17 for each 887 miRNA for specific cell ontology clusters were not corrected for multiple testing. 888

889 Identification of miRNA promoters

Candidate pri-miRNAs consisted of transcripts annotated in Gencode⁶¹ v19 (human) 890 or vM5 (mouse) or in the NCBI Entrez Gene database⁶². For each pre-miRNA, we 891 892 selected all candidate pri- miRNAs with a transcription start site upstream of the pre-893 miRNA and a 3' end downstream of the 5' end of the pre-miRNA, and defined all FANTOM5 permissive CAGE peaks¹⁷ within the genomic region from 500 bp 894 895 upstream of the 5' end of the pri-miRNA to the 5' end of the pre-miRNA as the set of 896 candidate promoters associated with the pre-miRNA. We averaged the expression 897 level (in tags-per-million) of each candidate promoter across all FANTOM5 CAGE 898 samples, and selected the candidate promoter with the highest average expression 899 level as the (computationally predicted) promoter of the miRNA. Each human 900 miRNA in the robust set was manually curated by two annotators.

901

902 Validation of miRNA promoters by RAMPAGE

We downloaded all 212 BAM files containing ENCODE RAMPAGE sequencing data mapped to human genome assembly hg19 that were not marked as "low read depth" or "low replicate concordance". We retained the 5' end positions of RAMPAGE transcripts with a 3' end within 1,000 basepairs of a pre-miRNA locus, discarding 5' end positions supported by fewer than 5 RAMPAGE transcripts, and associated the remaining 5' end positions with the pre-miRNA as putative transcription start sites.

910 Validation of miRNA promoters by RACE

We mixed 4.0 μl 5X First-Strand Buffer, 0.5 μl DTT (100 mM; Invitrogen, catalog
number 70726), 1.0 μl dNTP Mix (20 mM), spun briefly in a microcentrifuge, and
kept at room temperature. We combined 1.0-10.0 μl with 1 μg total RNA from
monocytes, macrophages, and dendritic cells, 1.0 μl Random Primer Mix (N-15) (20

915 μ M), and 0-9 μ l sterile water to reach a total volume of 11.0 μ l in separate 916 microcentrifuge tubes, mixed the contents and spun the tubes briefly. We incubated 917 these tubes at 72 °C for 3 minutes, and then cooled to 42 °C for 2 minutes. After 918 cooling, we spun the tubes for 10 seconds at 14,000 g to collect the contents at the 919 bottom. Next, we added 1.0 μ l of Smarter oligo (20 μ M) per reaction, and mixed well 920 by vortexing and spun the tube briefly in a microcentrifuge. We then added 0.5 ul 921 RNase Inhibitor (40 U/µl; Invitrogen RNaseOUT[™], catalog number 10777019) and 922 2.0 µl SMARTScribe Reverse Transcriptase (100 U; Clontech, catalog number 923 639537) to the buffer mix, and mixed these reagents at room temperature. Next, we 924 added 8.0 µl of the master mix to the RNA solution, mixed the contents of the tubes 925 by gently pipetting, and spun the tubes briefly. We incubated the tubes at 42 °C for 90 926 minutes and heated the tubes at 70 °C for 10 minutes in a hot-lid thermal cycler. We 927 then added 90 µl Tricine-EDTA buffer to each tube.

928 We prepared the master mix for the first PCR by combining 2.5 μ l of the cDNA 929 solution, 5.0 µl 10X Advantage 2 PCR buffer (Clontech, catalog number 639207), 1.0 930 µl dNTP Mix (10mM each) 50X Advantage 2 Polymerase Mix (Clontech), 1.0 µl of 931 the smarterRACE forward primer at 10 pmol/µl, 1.0 µl of the miRNA-specific outer 932 primer (Table S18) at 10 pmol/ μ l, and added PCR-grade water to reach a volume of 933 50 μ l. We ran a 2-step PCR program consisting of 1 minute at 95 °C, 25 cycles of 30 934 seconds at 95 °C followed by 70 seconds at 68 °C, 7 minutes at 68 °C, and finishing 935 at 8 °C. We diluted 5 µl of the primary PCR product into 245 µl of Tricine-EDTA 936 buffer.

We prepared the master mix for the second PCR by combining 5.0 µl of the product
of the first PCR after dilution with 5 µl of the 10X Advantage 2 PCR buffer, 1.0 µl
dNTP Mix (10 mM), 1.0 µl of 50X Advantage 2 Polymerase Mix (Clontech), 2.0 µl of

the Nextera_i7 primer, 2.0 µl of the miRNA-specific inner primer (Table S18), and 34
µl of PCR-grade water. We ran a 2-step PCR program consisting of 1 minute at 95 °C,
20 cycles of 30 seconds at 95 °C followed by 70 seconds at 68 °C, 7 minutes at 68 °C,
and finishing at 8 °C. We diluted 5 µl of the PCR product into 245 µl of TricineEDTA buffer.

945 We prepared the master mix for the third PCR by combining 5.0 µl of the PCR 946 product of the second PCR with 5.0 µl of 10X Advantage 2 PCR buffer, 1.0 µl dNTP 947 mix (10 mM), 1.0 µl of 40X Advantage 2 Polymerase Mix (Clontech), 2.0 µl of the 948 Nextera i7 primer, 2.0 µl of the Nextera i5 primer, and 34 µl of PCR-grade water. 949 We purified by AMPure at a 1.8 ratio, checked 2 μ l of the second PCR product on a 950 TapeStation, kept the libraries at -20 °C until sequencing, and pooled the PCR 951 products, each with a different barcode combination before paired-end sequencing on 952 a MiSeq sequencer (Illumina).

We mapped the sequencing data to the human genome using Blat⁶³, merged each pair
into a single mapped transcript, and retained transcripts that overlap an inner primer.

955 The histograms in Figure S21 show the position of the 5' end of these transcripts.

956

957 Promoter sequence conservation analysis

We previously compiled a list of transcription factors in human and mouse¹⁷. Proteincoding genes and lncRNAs consisted of all other genes annotated in the NCBI Entrez Gene database⁶² as protein coding or miscRNA, respectively. For each gene in these three categories, we selected the associated p1 CAGE peak as defined previously¹⁷ as the gene promoter, and discarded all genes without an associated CAGE peak. We then found the phastCons conservation score³⁶, obtained from the UCSC Genome Browser database⁶⁴, for the alignment of 99 vertebrate organisms against the human genome hg19, as a function of position relative to the transcription start site for each

gene and miRNA, and averaged these scores for each category at each position.

967

968 Construction of the FANTOM5 miRNA expression atlas of miRNAs

CAGE tag start site (CTSS) files³¹, excluding universal and whole body RNA 969 970 samples, were downloaded from http://fantom.gsc.riken.jp/5/datafiles/latest/basic/. 971 CAGE tag counts for technical replicates of the same RNA sample were summed for each genomic position. CAGE libraries published by Fort et al.¹⁹ were downloaded 972 973 from DDBJ, accession DRA000914. The number of CAGE tags at each genome 974 position were counted to generate CTSS files, and pri-miRNA expression tables were 975 generated by summing the CAGE tags under each promoter, calculating the total 976 number of tags mapped to the genome, and using this number to normalize to tags per 977 million (tpm).

Mature miRNA expression tables were generated by counting the number of sRNAtags to each miRNA locus, calculating the total number of tags mapping to the robust

980 miRNAs, and using this number to normalize to counts per million (cpm).

981 The CAGE and sRNA expression tables are available for download at the miRNA982 expression viewer at

983 http://fantom.gsc.riken.jp/5/suppl/De Rie et al 2017/

To generate the heatmap, we averaged the cpm-normalized expression values of each miRNA across donors for each cell type, and converted the expression profile of each miRNA to Z-scores by subtracting the mean and dividing by the standard deviation across cell types. The heatmap was sorted both for cell types and for miRNAs by performed centroid-linkage hierarchical clustering, using the Pearson correlation as the similarity measure.

991 Motif activity response analysis (MARA)

992 The genome-wide predictions of transcription factor binding sites were produced as described previously¹⁸. Briefly, we downloaded the whole-genome alignment of the 993 994 human genome hg19 against 99 other vertebrate genomes, and of the mouse genome 995 mm9 against 29 other vertebrate genomes, from the UCSC Genome Browser 996 database⁶⁴, and extracted the multiple alignments of human, macaque, mouse, rat, 997 cow, horse, dog, opossum, and chicken. We divided the genome into segments and realigned each segment using T-Coffee⁶⁵, and generated genome-wide transcription 998 factor binding site (TFBS) predictions using MotEvo⁶⁶ for the SwissRegulon set of 999 position-weight matrix motifs⁶⁷ (Figure S29a). We then counted the number of 1000 1001 predicted TFBSs for each motif in the -300 to +100 base pair base proximal promoter regions of genes in the NCBI Entrez Gene database⁶², excluding all miRNA 1002 promoters (Figure S29b). Next, we used MARA³⁸ to decompose the FANTOM5 1003 1004 CAGE expression profiles of these promoters in terms of their associated motifs, 1005 vielding the activity profile of each motif across the FANTOM primary samples 1006 (Figure S29c). We then counted the number of TFBSs for each motif in the -300 to +1007 100 base pair base proximal promoter region of each miRNA (Figure S29d), and 1008 predicted the miRNA expression level by calculating the weighted sum of the 1009 activities for motifs found (Figure S29e). We compared the predicted expression 1010 levels to the expression levels of the mature miRNA observed in the FANTOM5 1011 sRNA sequencing data (Figure S29f) and calculated their correlation (Figure S29g) as 1012 a measure of the accuracy of the miRNA promoter identification. Following the MARA procedure³⁸, we normalized the cpm expression values of miRNAs by adding 1013 1014 0.5, taking the base-2 logarithm, subtracting the mean across samples, and finally

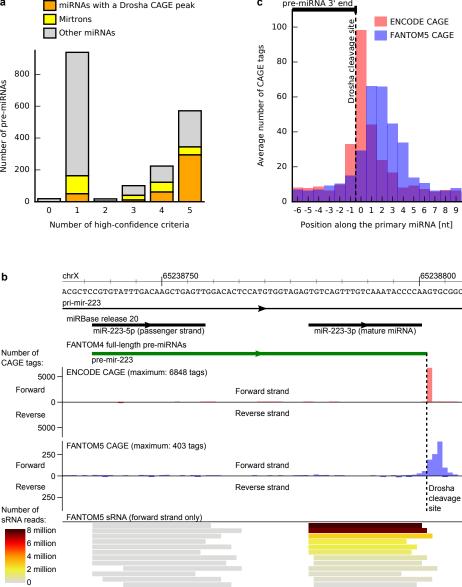
- 1015 subtracting the mean across miRNAs. We defined strongly differentially expressed
- 1016 miRNAs, included in Figure S20d and S20e, as those that had a standard deviation in
- 1017 expression, after normalization, across samples larger than 2.
- 1018
- 1019 Data availability
- Raw sequencing data of the sRNA libraries are available at the DNA Data Bank of
 Japan (DDBJ; http://www.ddbj.nig.ac.jp/) under accession numbers DRA001101,
 DRA002711, DRA003804, and DRA003807, and for the RACE experiments at the
 NCBI Gene Expression Omnibus (NCBI GEO; https://www.ncbi.nlm.nih.gov/geo/)
 under accession number GSE98695.
- 1025

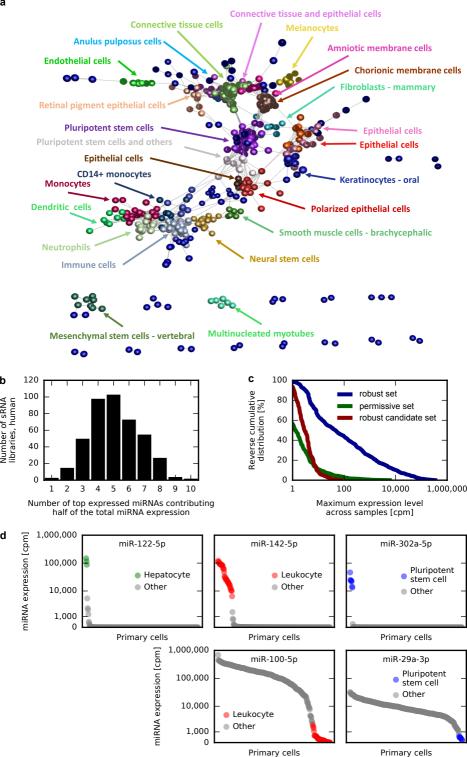
1026 Supplemental references

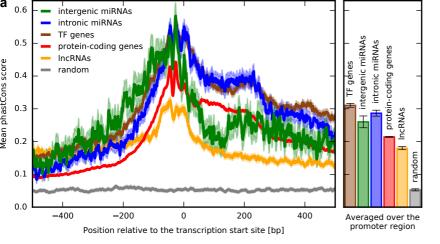
- 1027 1028
- 45. Abugessaisa, I., *et al.* FANTOM5 transcriptome catalog of cellular states
 based on Semantic MediaWiki. *Database (Oxford)* 2016, baw105 (2016).
- 46. Lassmann, T., Hayashizaki, Y. & Daub, C.O. TagDust—a program to
 eliminate artifacts from next generation sequencing data. *Bioinformatics* 25,
 2839–2840 (2009).
- 47. Li, H. & Durbin, R. Fast and accurate short read alignment with BurrowsWheeler transform. *Bioinformatics* 25, 1754–1760 (2009).
- 48. De Hoon, M.J.L. *et al.* Cross-mapping and the identification of editing sites in
 mature microRNAs in high-throughput sequencing libraries. *Genome Res.* 20,
 257–264 (2010).
- 1039 49. Lorenz, R. et al. ViennaRNA Package 2.0. Algorithms Mol. Biol. 6, 26 (2011).

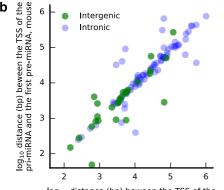
- 1040 50. Vijayan, D., Radford, K.J., Beckhouse, A.G., Ashman, R.B. & Wells, C.A.
- 1041 Mincle polarizes human monocyte and neutrophil responses to *Candida* 1042 *albicans. Immunol. Cell Biol.* **90**, 889–895 (2012).
- 1043 51. Busk, P.K. A tool for design of primers for microRNA-specific quantitative
 1044 RT-qPCR. *BMC Bioinformatics* 15, 29 (2014).
- 1045 52. Schwarzenbach, H., Da Silva, A.M., Calin, G. & Pantel, K. Data
 1046 normalization strategies for microRNA quantification. *Clin. Chem.* 61, 1333–
 1047 1342 (2015).
- 1048 53. Nagpal, N. & Kulshreshtha, R. miR-191: an emerging player in disease
 1049 biology. *Front. Genet.* 5, 99 (2014).
- 54. Moon, H.G., Yang, J., Zheng, Y. & Jin, Y. miR-15a/16 regulates macrophage
 phagocytosis after bacterial infection. *J. Immunol.* 193, 4558–4567 (2014).
- 1052 55. Vinod, M., et al. miR-206 controls LXRα expression and promotes LXR-
- 1053 mediated cholesterol efflux in macrophages. *Biochim. Biophys. Acta* 1841,
 1054 827–835 (2014).
- 1055 56. Cobos Jiménez, V., *et al.* Next-generation sequencing of microRNAs in
 1056 primary human polarized macrophages. *Genom. Data* 2, 181–183 (2014).
- 1057 57. Zhang, L., *et al.* miR-153 supports colorectal cancer progression via
 1058 pleiotropic effects that enhance invasion and chemotherapeutic resistance.
 1059 *Cancer Res.* 73, 6435–6447 (2013).
- 1060 58. Srivastava, S.K., *et al.* MicroRNA-345 induces apoptosis in pancreatic cancer
- 1061 cells through potentiation of caspase-dependent and -independent pathways.
- 1062 Br. J. Cancer 113, 660–668 (2015).

- 1063 59. Robinson, M.D., McCarthy, D.J. & Smyth, G.K. edgeR: a Bioconductor
- package for differential expression analysis of digital gene expression data. *Bioinformatics* 26, 139–140 (2010).
- 1066 60. Anders, S. & Huber, W. Differential expression analysis for sequence count
 1067 data. *Genome Biol.* 11, R106 (2010).
- 1068 61. Harrow, J. *et al.* GENCODE: the reference human genome annotation for The
 1069 ENCODE Project. *Genome Res.* 22, 1760–1774 (2012).
- 1070 62. Brown, G.R. *et al.* Gene: a gene-centered information resource at NCBI.
 1071 *Nucleic Acids Res.* 43, D36–D42 (2015).
- 1072 63. Kent, W.J. BLAT—The BLAST-like Alignment Tool. *Genome Res.* 12, 656–
 1073 664 (2002).
- 1074 64. Karolchik, D. *et al.* The UCSC Genome Browser database: 2014 update.
 1075 *Nucleic Acids Res.* 42, D764–D770 (2014).
- 1076 65. Notredame, C., Higgins, D.G. & Heringa, J. T-Coffee: A novel method for fast
 1077 and accurate multiple sequence alignment. *J. Mol. Biol.* 302, 205–217 (2000).
- 1078 66. Arnold, P., Erb, I., Pachkov, M., Molina, N. & Van Nimwegen, E. MotEvo:
- integrated Bayesian probabilistic methods for inferring regulatory sites and
 motifs on multiple alignments of DNA sequences. *Bioinformatics* 28, 487–494
 (2012).
- 1082 67. Pachkov, M., Balwierz, P.J., Arnold, P., Ozonov, E. & Van Nimwegen, E.
 1083 SwissRegulon, a database of genome-wide annotations of regulatory sites:
 1084 recent updates. *Nucleic Acids Res.* 41, D214–D220 (2013).
- 1085









 \log_{10} distance (bp) beween the TSS of the pri-miRNA and the first pre-miRNA, human

